Adv. Manuf. (2018) 6:95–106
https://doi.org/10.1007/s40436-018-0210-4

Chatter stability prediction in high-speed micromilling of Ti6Al4V via finite element based microend mill dynamics

Kundan K. Singh[1] · **Ramesh Singh**[1]

Received: 22 December 2016 / Accepted: 4 January 2018 / Published online: 3 February 2018

Abstract High-speed micromilling (spindle speeds 100 000 r/min) can create complex three-dimensional microfeatures in difficult-to-machine materials. The micromachined surface must be of high quality, to meet functional requirements. However, chatter-induced dynamic instability deteriorates the surface quality and can be detrimental to tool life. Chatter-free machining can be accomplished by identifying stable process parameters via stability lobe diagram. To generate accurate stability lobe diagram, it is essential to determine the microend mill dynamics. Frequency response function is required to determine the tool-tip dynamics obtained by experimental impact analysis. Note that application of impact load at the microend mill tip (typically 100 – 500 μm) is not feasible as it would invariably end with tool failure. Consequently, alternative methods need to be developed to identify the microend mill dynamics. In the present work, the frequency response function for the microend mill is obtained by finite element method modal analysis. The frequency response function obtained from modal analysis has been verified from the experimentally obtained frequency response function. The experimental frequency response function was obtained by impacting the microend mill near the taper portion with an impact hammer and measuring the vibration of the tool-tip with a laser displacement sensor. The fundamental frequency obtained from finite element method modal analysis shows a difference of 6.6% from the experimental fundamental frequency. Microend mill dynamics obtained from the finite element method is used for chatter prediction in high-speed micromilling operations. The stability lobe diagram predicts the stability boundary accurately at 60 000 r · min^{-1} and 80 000 r/min; however, a slight deviation is observed at 100 000 r/min.

Keywords Chatter · Micromilling · Microend mill dynamics · Frequency response function · Finite element modal analysis

1 Introduction

The demand for microcomponents is increasing owing to the continuous push for miniaturization. These microcomponents or features with complex geometry can be manufactured by a micromilling process in a wide range of engineering materials, such as metals, polymers, and ceramics [1]. These microcomponents find application in consumer electronics, automobiles, defense, space-flight instruments, and bio-medical devices, etc. [1–3]. One of the challenges of micromilling is the limited stiffness of the microend mill, which makes it highly susceptible to failure, especially during micromachining of high strength low diffusivity materials like Ti and Ni-alloys. One way of overcoming this limitation is to reduce the chip load by using very high spindle speeds.

The chip loads (feed/flute) in high-speed micromilling can be close to the tool edge radius and critical chip thickness (minimum chip thickness for chip formation), which affects the cutting mechanics. It can lead to intermittent chip formation and ploughing/rubbing takes place instead of shearing [4]. In addition, the run-out and misalignment effects lead to fluctuation in the cutting forces. This effect is accentuated and often observed at relatively small force magnitudes owing to low chip loads

✉ Kundan K. Singh
kundanju@gmail.com

[1] Department of Mechanical Engineering, Indian Institute of Technology Bombay, Powai, Mumbai 400076, India

that cause dynamic instability. If not controlled, this dynamic instability can lead to surface deterioration and catastrophic tool failure. Chatter is a self-excited vibration that occurs because of the interaction between the tool and the workpiece. The chatter phenomenon occurs because of the regenerative effect on the machined surface between two consecutive tooth passes [5].

Chatter can be avoided by machining at stable process parameters given by stability lobe diagrams. It may be noted that the stability lobe diagram (SLD) is a function of the dynamics and kinematics of the chip formation process. Hence, the accuracy of the SLD depends on accurate determination of cutting coefficients and tool tip dynamics. Tool tip dynamics (natural frequencies, stiffness and damping coefficients) are derived from the frequency response function (FRF) at the tip of a microend mill. The FRF for a macro end mill can be obtained by experimental modal analysis relatively easily, but experimental modal analysis for determining the tool-tip dynamics of a microend mill is not feasible. Note that impacting the tip of the microend mill with an impact hammer will invariably damage the tool. In addition, accelerometers, because of their weight, cannot be used for measuring the response at the tip. Consequently, an alternative method like receptance coupling, finite element (FE)-based modal analysis, and shaker and piezo actuator-based experimental modal analysis must be used. Many researchers have used the receptance coupling method [6–11] to determine the tool-tip dynamics for a microend mill. A microend mill with spindle collet is divided into two substructures: the first substructure contains the collet and a part of the shank of the end mill, and the second substructure contains the remaining part of the shank with a taper portion of the tool and the cutting edge [6]. The FRF of the first substructure is determined experimentally, whereas finite element analysis is required for the second substructure with a free-free beam boundary condition wherein the higher modes are needed to compute the FRF of the tool [12]. The receptance coupling method also assumes rigid and spring-damper connections between the substructures, which can affect the accuracy of tool-tip dynamics. In addition, the difficulty in determining higher modes and the experimental error induced because of noise can adversely affect the composite FRF determined via receptance coupling. However, FRF can also be determined by impacting the microend mill at different positions other than the tip and measuring the displacement at the tool-tip via a non-contact sensor like a displacement sensor [13, 14]. Jin and Altintas [2] determined the tool tip dynamics for a microend mill by exciting the shank of the tool with a piezoelectric actuator. The excited force was measured by a tri-axial load cell glued to a fixture clamped on the *x*-*y* stages, and the tool displacement was measured with a laser Doppler vibrometer. However, these experiments need to be repeated for each overhang length of the tool.

Experimental modal analysis requires repetition for different cutting tool geometry, which is time consuming and costly, specifically for the manufacturing industry [15], and the receptance coupling method also suffers from many drawbacks. To overcome these difficulties in obtaining the tool tip dynamics for a microend mill, an alternative approach based on finite element modal analysis has been adopted in the present work.

The FRF obtained here has been validated experimentally. The validated FRF obtained from the FE modal analysis is used in stability analysis of a two degree of freedom model, which represents the micromilling process. Cutting coefficients for the shearing zone have been identified by carrying out the experiment at different uncut chip thicknesses. The theoretical SLD has been validated with micromilling experiments on Ti6Al4V at different machining parameters.

2 Micromilling process model

The micromilling process is modeled as a two degree of freedom mass, spring and damper system as shown in Fig. 1. The tangential (F_{tj}) and radial forces (F_{rj}) at the tool tip for tooth j are given as

$$\begin{cases} F_{tj} = K_{tc} a h(\phi_j), \\ F_{rj} = K_r F_{tj}, \end{cases} \tag{1}$$

where K_{tc} and K_r are the tangential cutting force coefficient and cutting constant, respectively. Instantaneous chip

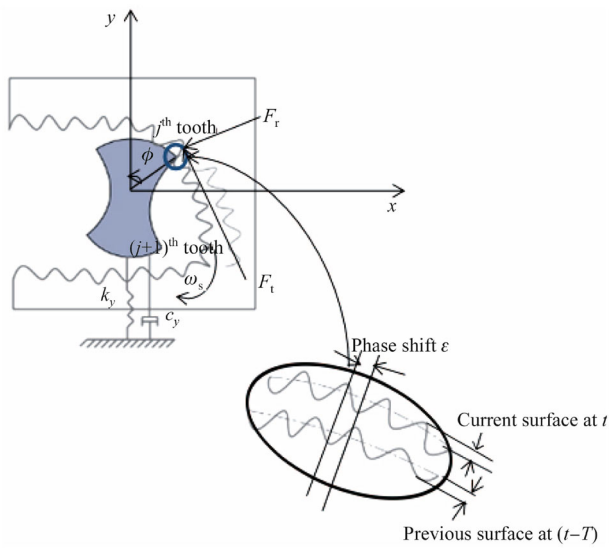

Fig. 1 Micromilling process model

thickness $h(\phi_j)$ is the dynamic chip thickness due to the regeneration effect, and a is the axial depth of cut.

Chatter modeling is carried out in the frequency domain. The characteristic equation of the closed loop dynamic milling system is given as [16, 17]

$$\det\left|\boldsymbol{I}-\frac{1}{2}K_{\mathrm{tc}}a\left(1-\mathrm{e}^{-\mathrm{i}\omega_{\mathrm{c}}T}\right)\boldsymbol{A}_0\boldsymbol{\Phi}(\mathrm{i}\omega_{\mathrm{c}})\right|=0, \tag{2}$$

where ω_{c} is the chatter frequency and $\omega_{\mathrm{c}}T$ is the phase difference of the cutting wave at successive tooth periods T. $\boldsymbol{A}_0$ is the time invariant but immersion dependent directional cutting coefficient matrix, which can be expressed as [16, 17]

$$\boldsymbol{A}_0=\frac{N}{2\pi}\begin{bmatrix}\alpha_{xx} & \alpha_{xy}\\ \alpha_{yx} & \alpha_{yy}\end{bmatrix}, \tag{3}$$

where the matrix elements are given as

$$\alpha_{xx}=\frac{1}{2}\left(\cos 2\emptyset-2K_{\mathrm{r}}\emptyset+K_{\mathrm{r}}\sin 2\emptyset\right)_{\emptyset_{\mathrm{st}}}^{\emptyset_{\mathrm{ex}}}, \tag{4}$$

$$\alpha_{xy}=\frac{1}{2}\left(-\sin 2\emptyset-2\emptyset+K_{\mathrm{r}}\cos 2\emptyset\right)_{\emptyset_{\mathrm{st}}}^{\emptyset_{\mathrm{ex}}}, \tag{5}$$

$$\alpha_{yx}=\frac{1}{2}\left(-\sin 2\emptyset+2\emptyset+K_{\mathrm{r}}\cos 2\emptyset\right)_{\emptyset_{\mathrm{st}}}^{\emptyset_{\mathrm{ex}}}, \tag{6}$$

$$\alpha_{yy}=\frac{1}{2}\left(-\cos 2\emptyset-2K_{\mathrm{r}}\emptyset-K_{\mathrm{r}}\sin 2\emptyset\right)_{\emptyset_{\mathrm{st}}}^{\emptyset_{\mathrm{ex}}}, \tag{7}$$

where $\emptyset$ is the immersion angle of the tooth measured clockwise from the y-axis, and $\emptyset_{\mathrm{st}}$ and $\emptyset_{\mathrm{ex}}$ are the entry and exit angles of the tooth relative to the workpiece. N is the total number of flutes of the microend mill. $\boldsymbol{\Phi}(\mathrm{i}\omega_{\mathrm{c}})$ is the FRF at the tool tip assuming a rigid workpiece, which is given by

$$\boldsymbol{\Phi}(\mathrm{i}\omega_{\mathrm{c}})=\begin{bmatrix}\Phi_{xx}(\mathrm{i}\omega) & \Phi_{xy}(\mathrm{i}\omega)\\ \Phi_{yx}(\mathrm{i}\omega) & \Phi_{yy}(\mathrm{i}\omega)\end{bmatrix}, \tag{8}$$

where $\Phi_{xx}(\mathrm{i}\omega)$ and $\Phi_{yy}(\mathrm{i}\omega)$ are the direct transfer functions in the x- and y- directions, respectively, and $\Phi_{xy}(\mathrm{i}\omega)$, and $\Phi_{yx}(\mathrm{i}\omega)$ are the cross transfer functions at the tool tip. These transfer functions at the tool tip are obtained by FE-based modal analysis in the present work. These transfer functions at the tool tip are expressed as

$$\Phi_{xx}(\mathrm{i}\omega)=\sum_{m=1}^{a}\frac{\omega_{n,y,m}^2}{K_{x,m}\left(\omega_{n,x,m}^2+2\zeta_{x,m}\omega_{n,m}\omega_{\mathrm{c}}-\omega_{\mathrm{c}}^2\right)}, \tag{9}$$

$$\Phi_{yy}(\mathrm{i}\omega)=\sum_{m=1}^{a}\frac{\omega_{n,y,m}^2}{K_{y,m}\left(\omega_{n,y,m}^2+2\zeta_{x,m}\omega_{n,y,m}\omega_{\mathrm{c}}-\omega_{\mathrm{c}}^2\right)}, \tag{10}$$

where $\omega_{n,y,m}$, $K_{x,m}$ and $\zeta_{x,m}$ are the natural frequency, stiffness and damping factor, respectively, of the microend mill for mode 1 to mode a.

Equation (2) can also be solved by finding its eigenvalue using MATLAB. This eigenvalue is obtained by the "eig" function through formulating Eq. (2) as

$$\det|\boldsymbol{\Phi}_0(\mathrm{i}\omega_{\mathrm{c}})-\Lambda\boldsymbol{I}|=0, \tag{11}$$

$$\text{where}\quad \Lambda=\frac{4\pi}{NaK_{\mathrm{tc}}\left(1-\mathrm{e}^{-\mathrm{i}\omega_{\mathrm{c}}T}\right)}, \tag{12}$$

$$\text{and}\quad \boldsymbol{\Phi}_0(\mathrm{i}\omega_{\mathrm{c}})=\frac{2\pi}{N}\boldsymbol{A}_0\boldsymbol{\Phi}(\mathrm{i}\omega_{\mathrm{c}}). \tag{13}$$

After calculating the eigenvalue Λ from Eq. (11), it can be put into Eq. (12), and then by equating the real and imaginary parts, a limited depth of cut is obtained as [20]

$$a_{\mathrm{lim}}=\frac{2\pi\Lambda_{\mathrm{Re}}}{NK_{\mathrm{tc}}\left(\Lambda_{\mathrm{Re}}^2+\Lambda_{\mathrm{Im}}^2\right)}\left(1+k^2\right), \tag{14}$$

where $k=\frac{\Lambda_{\mathrm{Im}}}{\Lambda_{\mathrm{Re}}}=\frac{\sin\omega_{\mathrm{c}}T}{1-\cos\omega_{\mathrm{c}}T}=\tan\psi$, and ψ is the phase shift of the eigenvalues. Tooth period T is given by $T=\frac{\varepsilon+2K\pi}{\omega_{\mathrm{c}}}$ and $\varepsilon=\pi-2\psi$, $K=0,1,2,3\cdots$. The spindle speed is given as

$$\omega_{\mathrm{s}}=\frac{60}{NT}. \tag{15}$$

Hence, it can be seen that the stability lobe diagram yields the maximum chatter free depth of cut at a given spindle speed and depends on the cutting coefficient and the tool tip dynamics.

3 Tool tip dynamics

Tool tip dynamics are required to obtain the chatter free depth of cut. Tool tip dynamics can be determined from the FRF at the tip of microend mill. The procedure for modeling and determining the FRF of the microend mill is shown in Fig. 2. This FRF is obtained by modal analysis wherein the microend mill is excited by a known force and the vibration of the tool tip is measured. The applied force and measured tool tip displacement are converted into frequency domain and the FRF is obtained by dividing the transformed displacement signature by the corresponding applied force. The microend mill and collet are modeled in ABAQUS® as a three-dimensional 8-node linear brick, reduced integration, hourglass control solid element (element type C3D8R) of non-uniform cross section, and 4-node doubly curved thin shell, reduced integration, hourglass control, finite membrane strains (element type S4R), respectively, as shown in Fig. 3. The dimensions of the cutting tool and collet chuck are shown in Fig. 4. The collet end is kept fixed by constraining all of its degrees of freedom. The overhang length of the tool is 20 mm and the remaining 18 mm of the shank is inserted into the collet. The tool tip is assumed as an equivalent cylinder with a

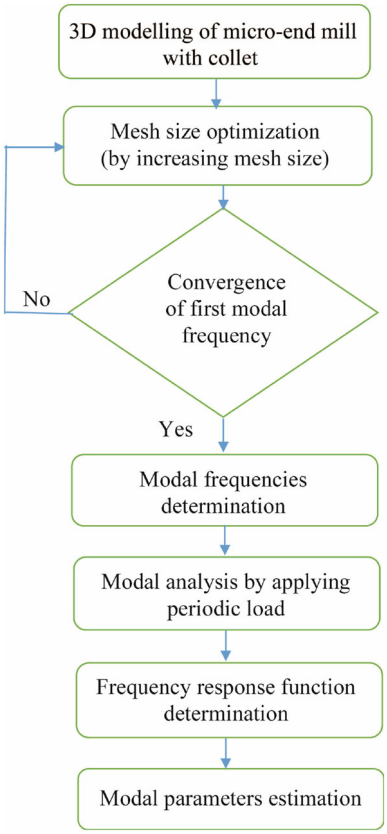

Fig. 2 Schematic diagram for modal analysis

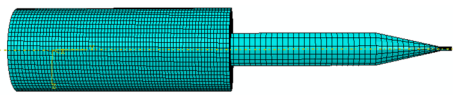

Fig. 3 Solid model of microend mill with collet

diameter that is 68% of the nominal diameter of the microend mill, to account for the cutting flutes [11]. To arrive at the optimal equivalent diameter, the authors have used different equivalent diameters and simulated the frequency response function. The closest match for the natural frequency with the experimental data has been obtained at 68% of the nominal diameter, also observed by Mascardelli et al. [11]. The properties of the tungsten carbide tool are as follows: density = 14 300 kg/m^2, Young's modulus = 580 GPa, Poisson's ratio = 0.28, and a damping ratio of 1.2% [7].

The collet is modeled such that it considers the compliance of the machine tool system. General contact includes all the nodes and edges in contact [18]. Surface interaction between the collet and cutting tool can enforce overclosure. Hence, surface interaction between the collet and cutting tool has been modeled as a general contact to avoid this initial overclosure. General contact also converges quickly compared to other interaction models [18]. Subsequent pressure overclosure during modal analysis was avoided through hard contact in normal behavior of interaction. Overclosure (h) depends on contact pressure (p) during the finite element analysis as per Eqs. (16) and (17) for hard contact [18]

$$p = 0 \text{ for } h < 0, \tag{16}$$

$$h = 0 \text{ for } p > 0. \tag{17}$$

In addition to this, general contact assumes that there is no penetration of the tool into the collet and only finite sliding takes place. However, frictionless motion has been assumed for the tangential interaction as the tool is excited normal to its axis. Damping has been used between the contact surfaces to allow the transmission of viscous pressure and shear stress to reduce the difficulties in convergence owing to sudden violation of the contact constraints [18].

A frictionless contact with a damping factor of 1.2% is defined between the collet and the tool. The run-out of 2 μm is given as clearance between the collet and the shank. An optimal mesh size has been obtained by using mesh sensitivity analysis. The mode shape frequency converges at about 29 170 elements, as shown in Fig. 5. Any further increase in the number of elements will not improve the results. Hence, the number of elements and nodes in the model are 29 170 and 20 919, respectively. The first three mode shapes and the corresponding natural frequencies are shown in Fig. 6.

After identifying the dominant modes, a harmonic load of 4 N has been applied at the tip of the tool in the modal

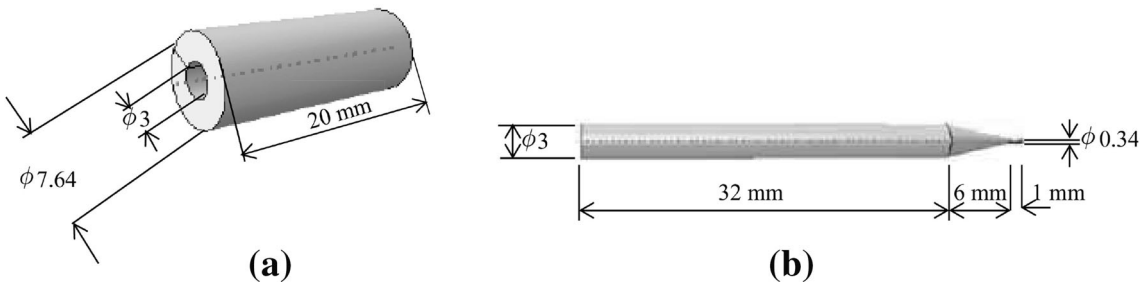

Fig. 4 Dimensions schematic diagram of **a** collet chuck, **b** cutting tool

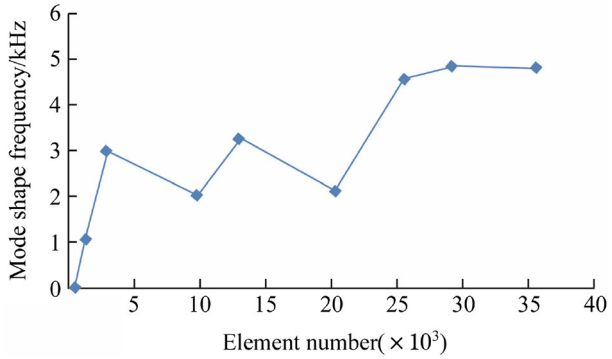

Fig. 5 Mesh sensitivity plot

analysis step and a corresponding displacement is obtained at the tip in the frequency domain. Note that the harmonic sinusoidal load depends on the extracted mode shape and the eigenfrequency of the structure. The equation of motion for the eigenmode α is given as [19]

$$\ddot{q}_\alpha + c_\alpha \dot{q}_\alpha + \omega_\alpha^2 q_\alpha = \frac{1}{m_\alpha}(f_{1\alpha} + \mathrm{i}f_{2\alpha})\exp(\mathrm{i}\Omega t) \tag{18}$$

where q_α, c_α, and ω_α are the amplitude, damping and undamped natural frequency, respectively, for eigenmode α, and m_α is the generalized mass of mode. The term $(f_{1\alpha} + \mathrm{i}f_{2\alpha})\exp(\mathrm{i}\Omega t)$ is the harmonic excitation given to the system. It can also be given in the form $(F_0 \cos \Omega t + \mathrm{i}F_0 \sin \Omega t)$, where F_0 is the amplitude of the force [19]. The FRF at the tip of the tool is obtained by

$$\Phi = \frac{X(\omega)}{F(\omega)}, \tag{19}$$

where $F(\omega)$ and $X(\omega)$ are the applied periodic load and corresponding displacement at the tool tip in the frequency domain, respectively. The real and imaginary part of the FRF at the tool tip is shown in Fig. 7.

The modal parameters, like natural frequency, stiffness and damping factor of the microend mill from FRF, were obtained by the peak picking method [20]. The dominant modes have been observed at 4 851 Hz ($\omega_{n,1}$), 5 081 Hz ($\omega_{n,2}$), and 7 170 Hz ($\omega_{n,3}$), which correspond to the three lowest points having negative values in the imaginary part of the FRF (see Fig. 7a). The damping ratios of the different modes of the tool tip are given by [20]

$$\begin{cases} \zeta_1 = \dfrac{\omega_5 - \omega_4}{2\omega_{n,1}}, \\ \zeta_2 = \dfrac{\omega_7 - \omega_6}{2\omega_{n,2}}, \\ \zeta_3 = \dfrac{\omega_9 - \omega_8}{2\omega_{n,3}}, \end{cases} \tag{20}$$

where ω_4, ω_5, ω_6, ω_7, ω_8 and ω_9 are the excited frequencies corresponding to three identified modes $\omega_{n,1}$, $\omega_{n,2}$ and $\omega_{n,3}$, respectively. Corresponding modal stiffnesses of the tool are given by

$$\begin{cases} K_1 = -\dfrac{1}{2A\zeta_1}, \\ K_2 = -\dfrac{1}{2B\zeta_2}, \\ K_3 = -\dfrac{1}{2C\zeta_3}, \end{cases} \tag{21}$$

where A, B and C are the negative peak values of the identified natural frequencies of all the three modes of the tool system. The modes of the microend mill with machine tool system compliance are shown in Table 1.

The obtained tool tip dynamics have been validated from the experimental modal analysis. Here, direct FRF determination at the tool-tip is not feasible owing to difficulties in exciting the microend mill tip. Consequently,

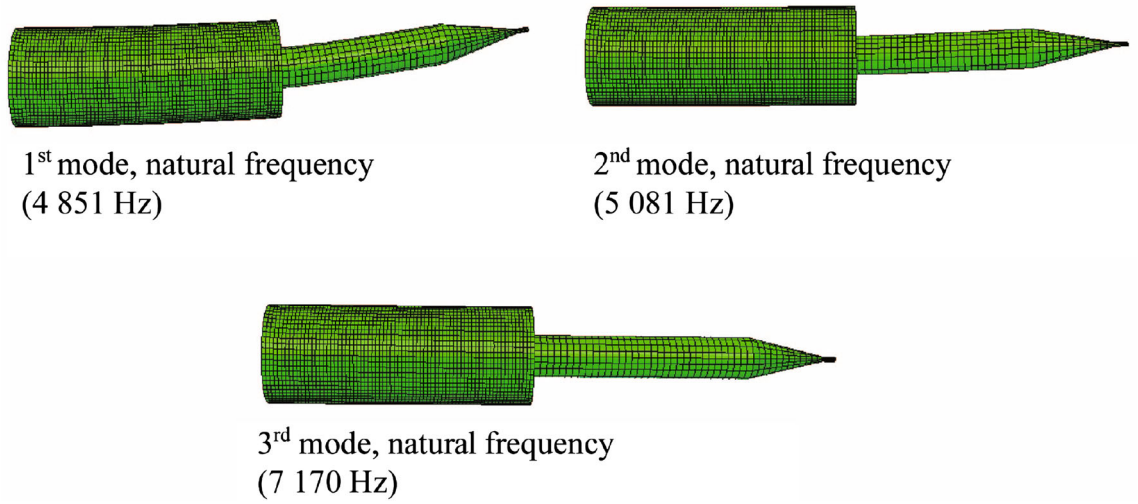

Fig. 6 Different modes of the microend mill

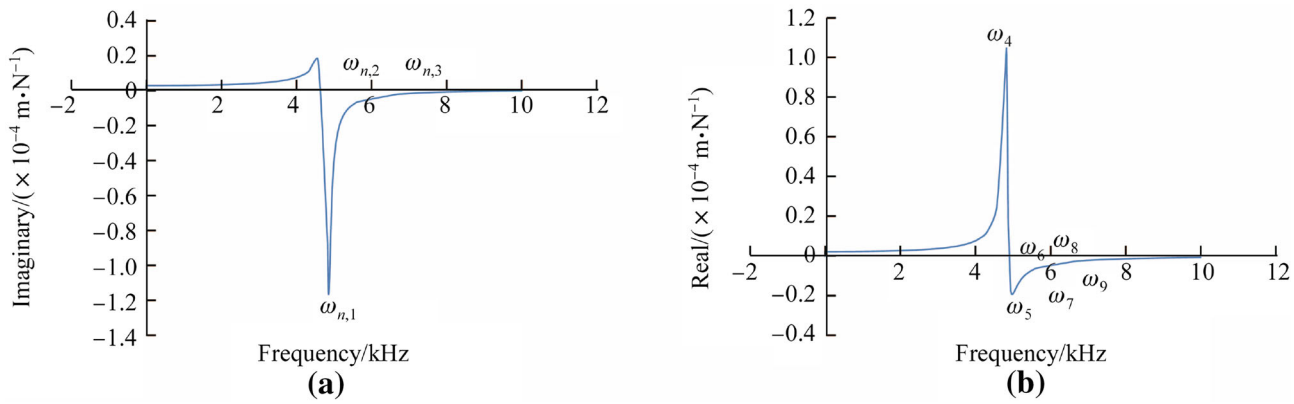

Fig. 7 Frequency response function at tool tip **a** imaginary part, **b** real part

Table 1 Tool tip dynamics

Mode	ω/Hz	K /(MN·m^{-1})	ζ
1	4 851	0.404	0.011
2	5 081	0.366	0.048
3	7 170	4.160	0.061

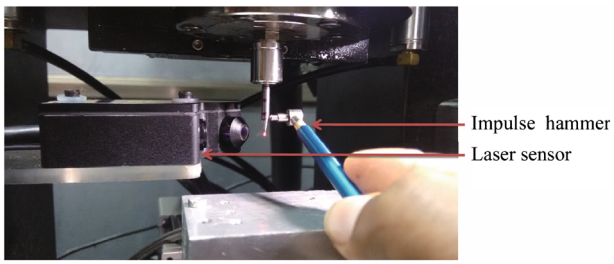

Fig. 8 Experimental set-up for modal analysis

excitation has been carried out near the tapered portion of the tool (see Fig. 8). Experimental modal analysis has been carried out by impacting the microend mill near the taper portion with an impact hammer (PCB, model 086E80) with a sensitivity of 22.5 mV/N, and by measuring the corresponding displacement of the tip of the microend mill. The displacement at the tip was measured by a laser displacement sensor (micro epsilon, LD 1607) with a sensitivity of 250 μm per 10 V and a spot diameter of 0.1 mm. The FRF of the tool-holder-spindle assembly is obtained by

$$\Phi_{xx}(\omega) = \frac{X(\omega)}{F(\omega)}, \tag{22}$$

where $X(\omega)$ is the measured response in the frequency domain and $F(\omega)$ is the impulse load applied in frequency on the tool. Experiments were repeated ten times and then the average of all the measured displacements and applied impulse loads in the frequency domain were used to obtain the FRF at the tool tip with minimum noise. The experimentally obtained imaginary and real parts of the frequency response function at the tool-tip with machine tool compliance are shown in Fig. 9. The experimentally obtained tool-tip dynamics are shown in Table 2.

An assumption of 68% equivalent diameter for the flute portion of the microend mill has been verified by error estimation between the first measured modal frequency and the simulated frequency at equivalent diameters of 50%, 68% and 90% of the microend mill diameter (500 μm). A minimum error of 6.59% for the 1st modal frequency was estimated between the simulation and experimental frequency response functions, which has been observed for an equivalent diameter of 68%, as shown in Fig. 10.

4 Determination of cutting coefficients

The tangential and radial cutting coefficients are determined by a series of slot cutting at depth of cut and cutting speed with varying feed per flute. *x*- and *y*-direction forces are measured and as an average value of the forces is approximately zero in magnitude, the root mean square (RMS) value of the forces for each condition can be calculated. Experimental set-up and details are presented in the proceeding section.

4.1 Experimental set-up

An ultra-high-speed micromachining center was developed in-house to carry out the microend milling operation. The high-speed spindle has a ceramic bearing and can rotate upto a maximum speed of 140 000 r/min and an average torque of 4.3 N·cm. The spindle is driven by an electric motor with a variable frequency drive. This three-axis micromachining center has stacked *x*-*y* stages, each having a ball screw driven by a DC brushless servo motor. The *x*-*y* stages have a positioning resolution of 0.5 μm and an

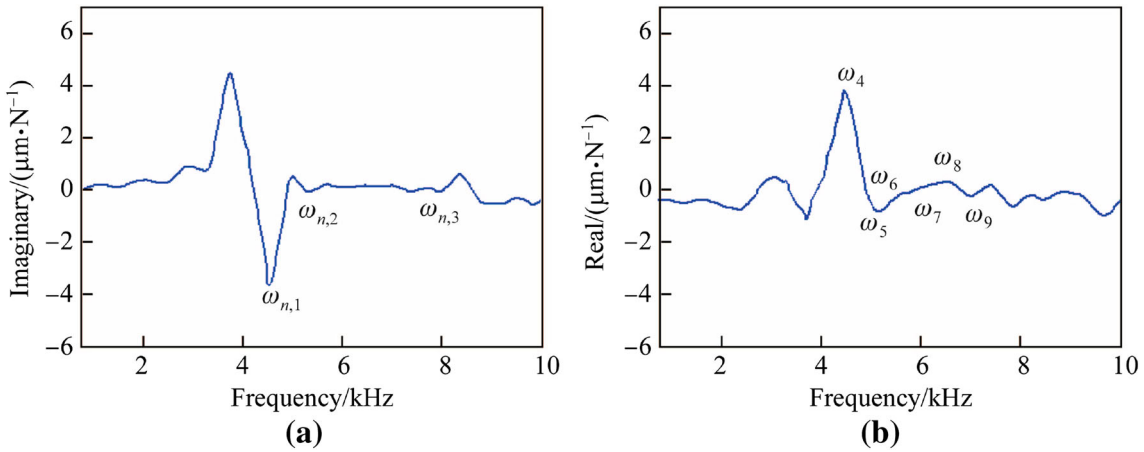

Fig. 9 Frequency response function of the tool with machine tool compliance **a** imaginary part, **b** real part

Table 2 Tool-tip dynamics (experimental)

Mode	ω/Hz	K/(MN·m^{-1})	ζ
1	4 551	2.11	0.064
2	5 332	108	0.036
3	7 383	167	0.023

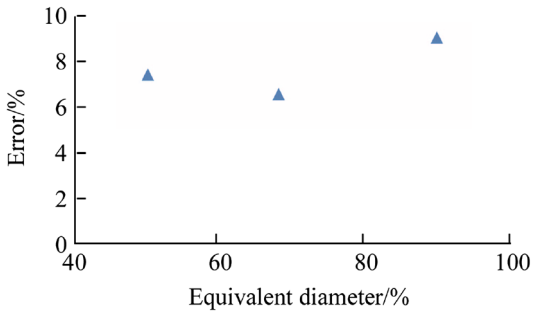

Fig. 10 Comparison of the first modal frequency for different equivalent diameters

accuracy of ± 1 μm. The *z*-stage has a pneumatically counter balanced linear motor stage with a positioning resolution of 5 nm. The micromachine was placed on a vibration isolation table. The set-up is shown in Fig. 11.

4.2 Experimental conditions

Slot milling was carried out on Ti6Al4V at a constant depth of cut and speed with varying feed/flute. A two fluted uncoated tungsten carbide tool, with a diameter of 500 μm, was used. All the experiments were done under dry conditions without any lubrication.

The edge radius of the cutting tool measured from the SEM image, shown in Fig. 12, was found to be 2.75 μm. The key geometric parameters of the tool are listed in Table 3. *x*- and *y*-directional forces were measured using a three-dimensional Kistler dynamometer (Minidyne 92561C1) connected to a data acquisition (NI DAQ) system.

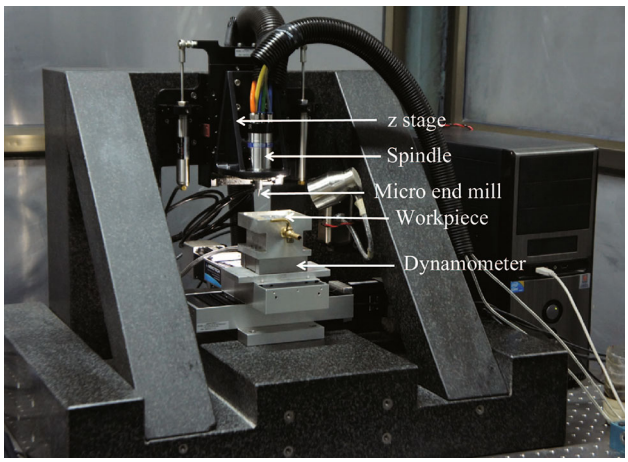

Fig. 11 Experiment set-up

4.3 Cutting coefficient determination

The averages of measured *x*- and *y*-directional cutting forces at each cutting condition can result in zero magnitude of the forces; hence, RMS values of the forces can be determined. The resultant RMS of *x*- and *y*-directional forces with corresponding feed/flute is shown in Fig. 13. The transition between ploughing and shearing occurs at a feed of 2.6 μm/flute, which is nearly equal to the edge radius of the tool, 2.75 μm.

The obtained *x*- and *y*-directional forces are transformed into tangential and radial forces. After calculating the RMS value of the tangential and radial forces, the cutting coefficient is obtained by linear fitment between the tangential

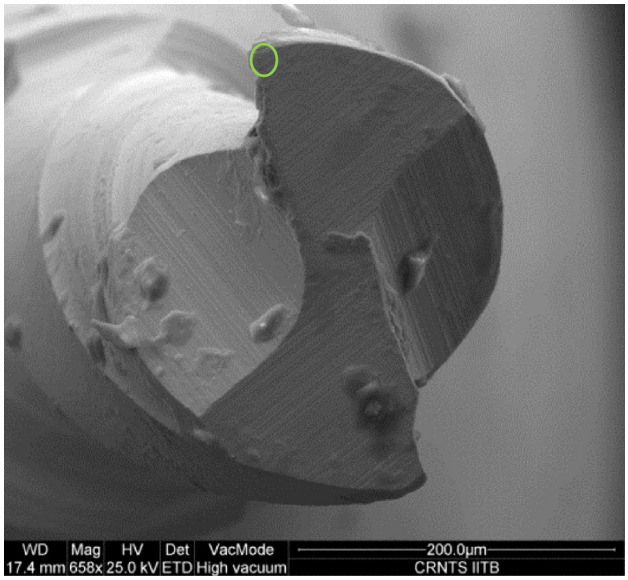

Fig. 12 Scanning electron micrograph of the 500 μm microtool

Table 3 Tool geometry

Parameter	Value
Tool shank diameter/mm	3
Tool diameter/μm	500
Tool edge radius/μm	2.75
Tool length/mm	38
Flute length/mm	1
Helix angle/(°)	30

and radial force per unit depth of cut and average chip thickness, as given by

$$F_{\mathrm{T}} = K_{\mathrm{tc}} a \bar{h}, \tag{23}$$

$$F_{\mathrm{R}} = K_{\mathrm{rc}} a \bar{h}, \tag{24}$$

where F_{T} and F_{R} are the RMS value of the tangential and radial forces, respectively. $\bar{h}$ is the average chip thickness which is a function of the immersion angle and the cutting conditions. For slot milling average chip thickness $\bar{h}$ for given feed per teeth (f_{t}) is defined as

$$\bar{h} = \frac{2}{\pi} f_{\mathrm{t}}. \tag{25}$$

The linear fitment is obtained by minimizing the square error

$$e = \sum_{q=1}^{n} \sum_{p=1}^{m} \left(F_{\mathrm{exp}q,p} - F_{\mathrm{theo}}\right)^2, \tag{26}$$

where n is the number of runs at each feed, and m is the number of selected samples for the analysis. F_{exp} and F_{theo} are the RMS values of experimental and theoretical forces, respectively.

Figures 14 and 15 show the linear fitment for tangential and radial cutting forces per unit depth cut with the average chip thickness, respectively. The obtained tangential and radial cutting coefficients are given in Table 4.

5 Results and discussion

The fundamental frequency (frequency of the first mode) determined from the finite element modal analysis shows a deviation of 6.6% from the fundamental frequency obtained by experimental modal analysis. Comparable fundamental frequencies (within 20% deviation) have been reported in the literature for the tool-tip dynamics of a 500 μm diameter tungsten carbide tool [6, 11]. This deviation can be attributed to the differences in machine tool compliance, tool holder geometry, and possibly tool geometry. A stability lobe diagram has been created for the obtained tool tip dynamics and cutting coefficient. This stability lobe diagram is obtained by plotting the limiting depths of cut (see Eq. (14)) at different spindle speeds (see Eq. (15)). The spindle speed is obtained from the tooth

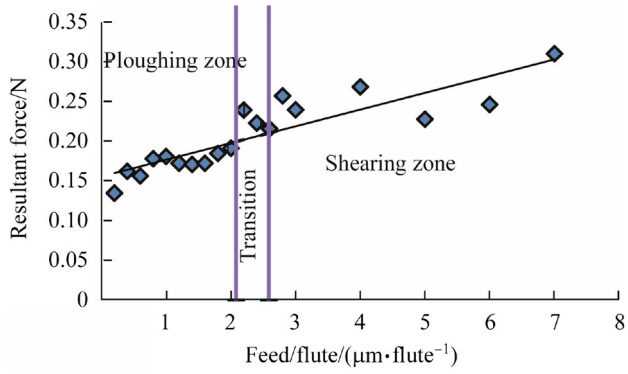

Fig. 13 Micromilling resultant forces at different feeds

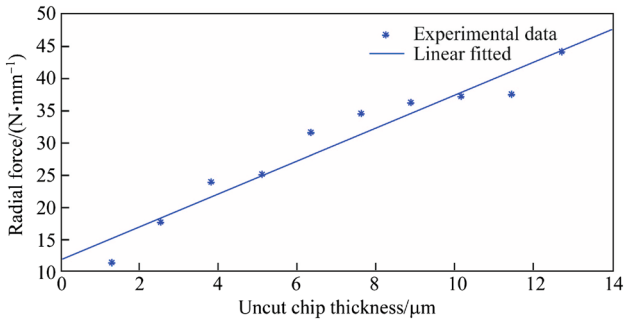

Fig. 14 RMS value of tangential forces at different uncut chip thickness for 80 000 r/min

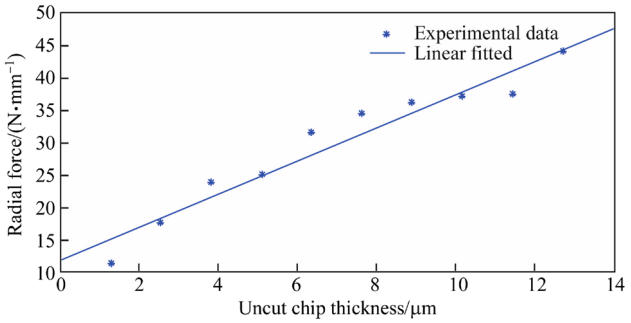

Fig. 15 RMS value of radial forces at different uncut chip thickness for 80 000 r/min

Table 4 Cutting coefficients for shearing zone

Coefficients	K_{tc}/(N·mm^{-2})	K_{rc}/(N·mm^{-2})
Ti6Al4V	2 800	2 500

passing period, which depends on the chatter frequency. The theoretical SLD plot is shown in Fig. 16.

The stability lobe diagram has been validated experimentally by the micromilling of Ti6Al4V at different process parameters. The cutting force signal obtained from the dynamometer cannot be used for stability analysis owing to its limited bandwidth [7, 11, 13, 21]. However, a displacement sensor accurately captures the dynamics of the high-speed micromilling operation [21]. Hence, vibration of a tool has been measured in the present work to analyze the dynamic stability of the micromilling operation. Vibration of the tool has been measured by the laser displacement sensor and the set-up is shown in Fig. 17. Machining has been carried out at spindle speeds of 60 000 r/min, 80 000 r/min and 100 000 r/min, with varying depth of cut.

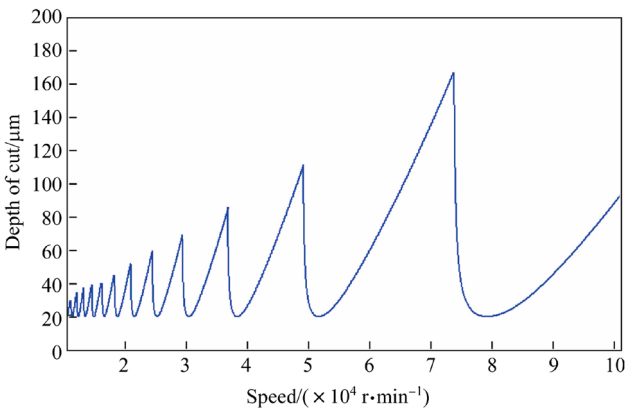

Fig. 16 Analytical stability lobe diagram

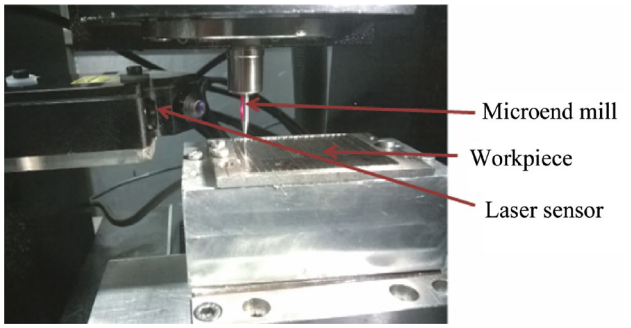

Fig. 17 Displacement sensor mounting for vibration measurement

Figure 18a shows the vibration signature in the frequency and time domains for a spindle speed of 80 000 r/min and a depth of cut of 20 μm. The vibration spectrum gives only the spindle rotational frequency (1 333 Hz), tooth passing frequency (2 666 Hz), and their harmonics; no dominant peak is observed near the tool natural frequency, and hence, stable cutting is achieved. The dominant vibration amplitude at 5 000 Hz, near the tool natural frequency (4 851 Hz), was observed for micromilling at 80 000 r/min spindle speed and 40 μm depth of cut (see Fig. 18b); this can be construed as chatter.

Similarly, at 100 000 r/min spindle speed and 20 μm depth of cut (see Fig. 19a), no chatter was observed owing to the absence of a dominant peak near the tool natural frequency. Only the spindle rotational frequency (1 666 Hz), tooth passing frequency (3 333 Hz), and their harmonics are dominant. However, chatter is observed at 100 000 r/min and 80 μm depth of cut owing to a higher amplitude near the tool natural frequency (4 851 Hz) (see Fig. 19 b).

Experimental validations were carried out at a high cutting velocity (157 mm/min for 100 000 r/min) and at lower uncut chip thickness (3 μm/flute), hence formation of the built-up edge is not conducive for these experimental conditions. Built-up edge formation typically occurs at lower cutting speeds. A fresh cutting tool was used to perform the experiment at each axial depth of cut and the tools were inspected periodically to ensure that wear and built-up edge formation had not taken place. Note that if tool wear and built up edge formation occurs, the tool-chip interface conditions alter, which has not been explicitly modeled in this work, and therefore the process dynamics will be affected. Consequently, care was taken to ensure that wear and built-edge formation did not occur in the experiment. Images of the tool with and without chatter are shown in Fig. 20, which show that the tool did not undergo significant wear.

The experimentally validated stability lobe diagram is shown in Fig. 21. There is a good agreement between the analytical and experimentally obtained stable process

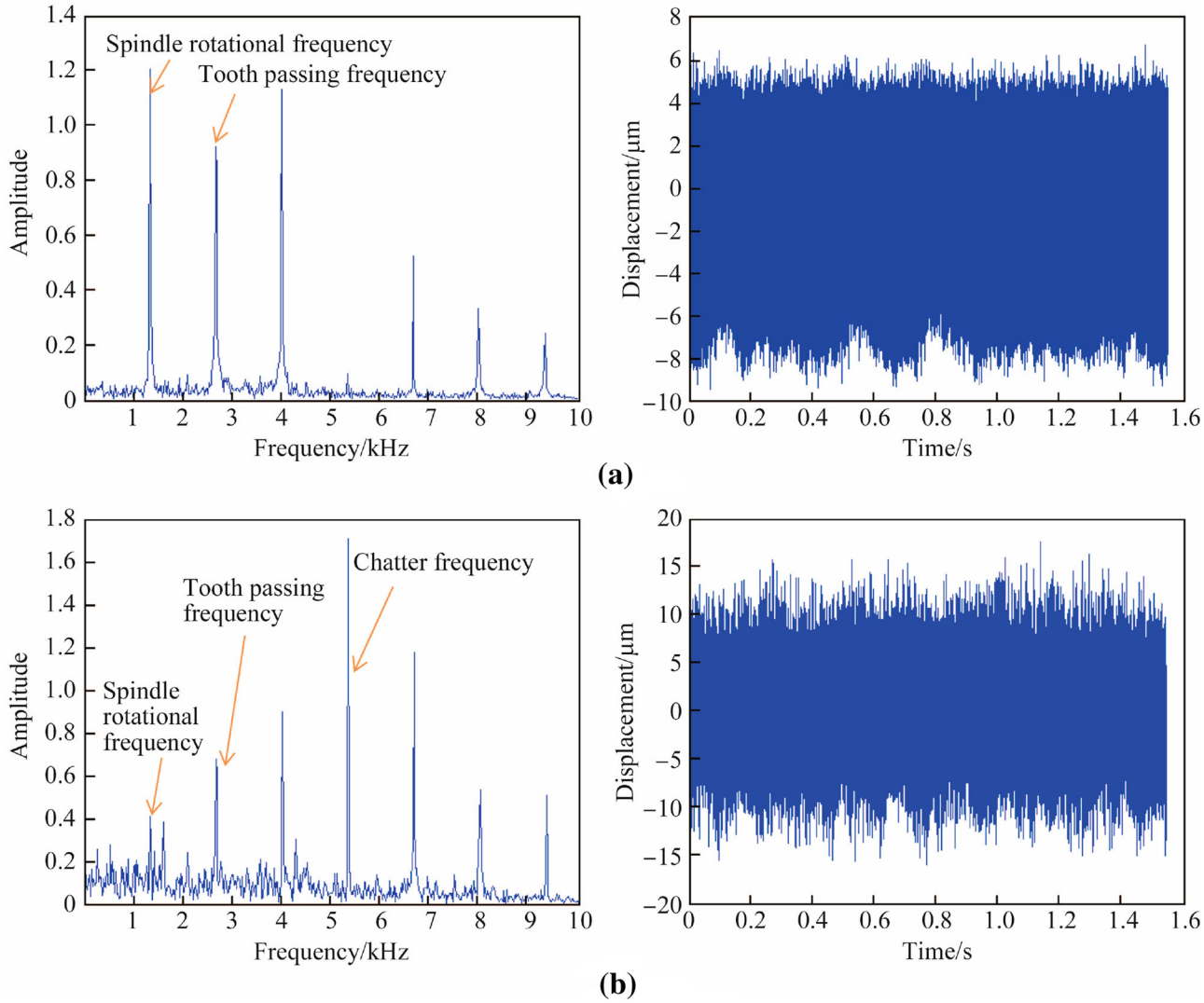

Fig. 18 Vibration signal in frequency domain and time domain at **a** spindle speed 80 000 r/min and depth of cut 20 μm, stable **b** spindle speed 80 000 r/min and depth of cut 40 μm, chatter

parameters. However, the assumption of constant cutting coefficient independent of cutting speed for ultra-high-speed machining stability gives an inaccurate prediction for stability lobe diagrams at 60 000 r/min and 100 000 r/min. Velocity-chip load dependent cutting coefficient had been developed to capture the high-speed micromilling process mechanics by Singh et al. [22]. A developed chatter model based on segmented cutting coefficient was shown to be more accurate, especially at higher speeds [22]. Hence, in the present work, stability prediction based on segmented cutting coefficient was carried out, as shown in Fig. 22. The Nyquist stability criterion was used to obtain this stability lobe diagram (see Fig. 22). There is a decrease in the predicted stable depth of cut at higher speeds (> 74 000 r/min) which was also observed during experiments. Hence, the segmented cutting coefficient captures some of the uncertainties of the micromilling process and predicts stability with reasonable accuracy.

6 Conclusions

In this paper, tool tip dynamics for a microend mill have been obtained from modal analysis based on the finite element method. The frequency response function at the tip of the tool is obtained by applying a harmonic load at the tip and measuring the corresponding displacement in the frequency domain. The frequency response function thus obtained appears to capture the tool-tip dynamics with reasonable accuracy without the complexities of receptance coupling. The theoretical SLD diagram is in good agreement with the experimental results. The following specific conclusions can be drawn from the present work.

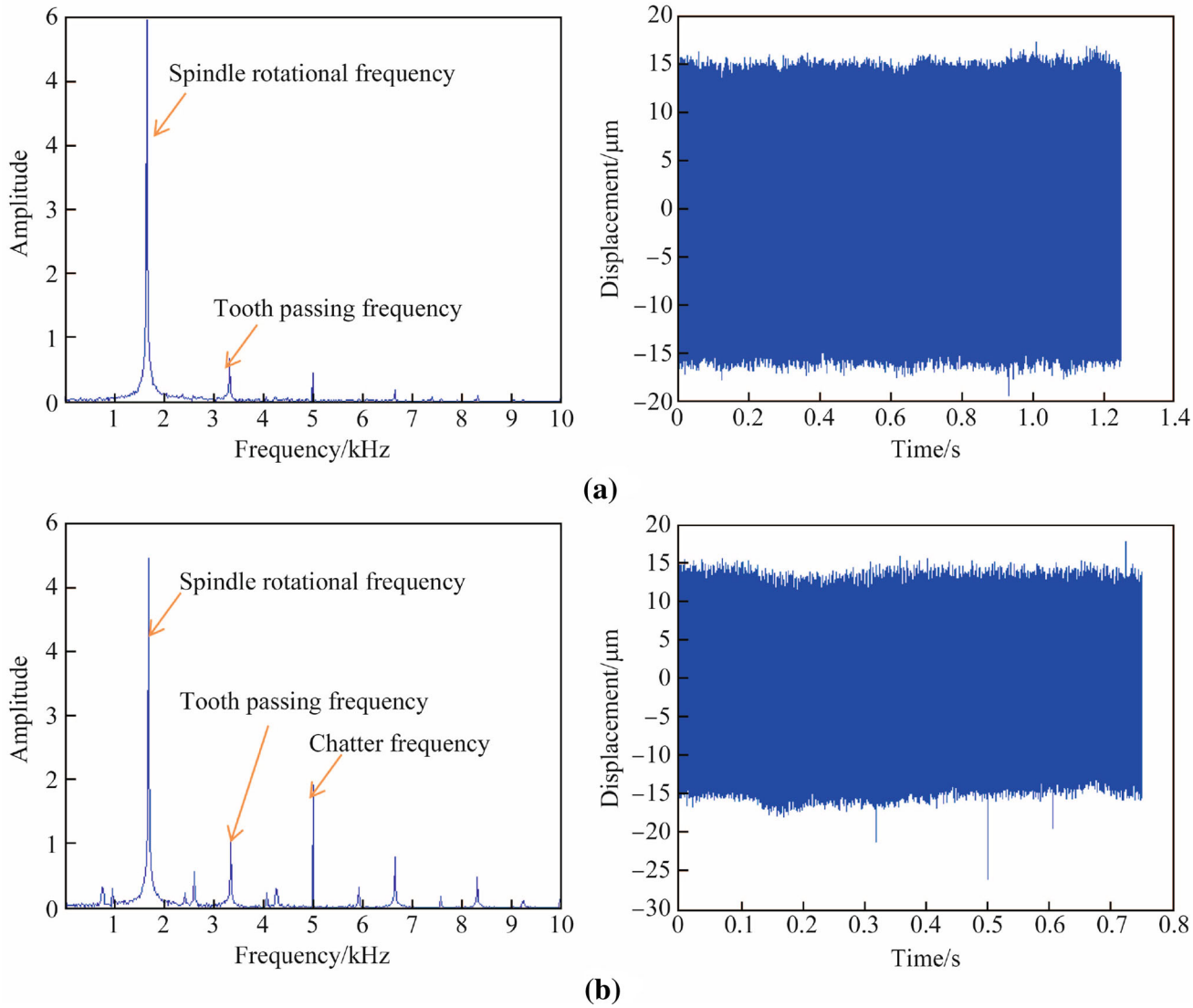

Fig. 19 Vibration signal in frequency domain and time domain at **a** spindle speed 100 000 r/min, depth of cut 20 μm, stable **b** spindle speed 100 000 r/min and depth of cut 80 μm, chatter

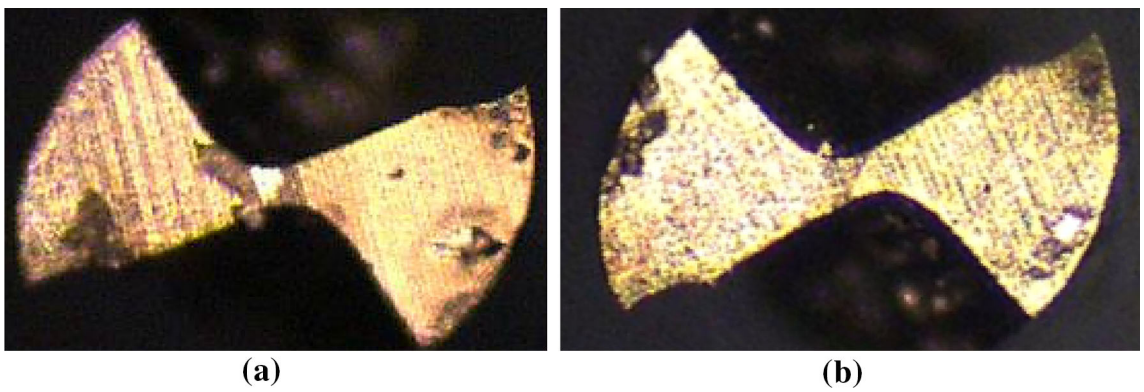

Fig. 20 Cutting tool image at spindle speed 80 000 r/min and depth of cut of **a** 20 μm (stable), **b** 60 μm (chatter)

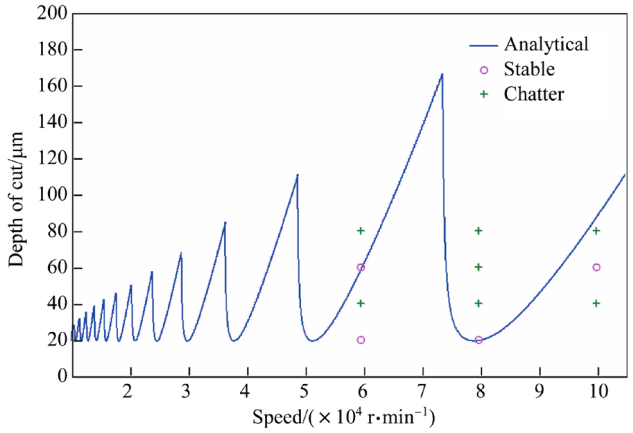

Fig. 21 Experimentally validated stability lobe diagram

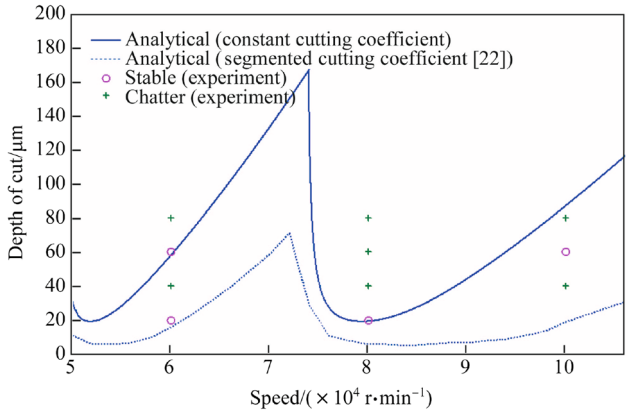

Fig. 22 Stability lobe diagram with segmented cutting coefficient

(i) Tool tip dynamics can be obtained from the finite element method modal analysis technique with reasonable accuracy.

(ii) The first mode natural frequency obtained from the finite element analysis approach shows 6.6% deviation from the natural frequency obtained experimentally.

(iii) The cutting coefficient captures the variation of RMS forces (force per unit depth of cut) with undeformed chip thickness. The root mean square errors for linear fitting of tangential and radial coefficient are 1.912 N/mm and 2.618 N/mm, respectively.

(iv) The analytical stability lobe diagram for the second degree of freedom micromilling model is in good agreement with experimental chatter conditions. The stability boundary is predicted accurately at 60 000 r/min and 80 000 r/min, and a slight deviation is observed at 100 000 r/min. This error is attributed to uncertainties in the determination of cutting coefficients.

References

1. Jun MB, DeVor RE, Kapoor SG (2006) Investigation of the dynamics of microend milling—part I: model development. J Manuf Sci Eng 128(4):893–900
2. Jin X, Altintas Y (2013) Chatter stability model of micro-milling with process damping. J Manuf Sci Eng 135(3):031011
3. Miao JC, Chen GL, Lai XM et al (2007) Review of dynamic issue in micro-end milling. Int J Adv Manuf Technol 31(9–10): 897–904
4. Ducobu F, Filippi E, Rivière-Lorphèvre E (2009) Chip formation and minimum chip thickness in micro-milling. In: Proceedings of the CIRP conference on modeling of machining operations, pp 339–346
5. Quintana G, Ciurana J (2011) Chatter in machining processes: a review. Int J Mach Tools Manuf 51(5):363–376
6. Graham E, Mehrpouya M, Nagamune R et al (2014) Robust prediction of chatter stability in micro milling comparing edge theorem and LMI. CIRP J Manuf Sci Technol 7(1):29–39
7. Rahnama R, Sajjadi M, Park SS (2009) Chatter suppression in micro end milling with process damping. J Mater Process Technol 209(17):5766–5776
8. Malekian M, Park SS, Jun MB (2009) Modeling of dynamic micro-milling cutting forces. Int J Mach Tools Manuf 49(7):586–598
9. Afazov SM, Zdebski D, Ratchev SM et al (2013) Effects of micro-milling conditions on the cutting forces and process stability. J Mater Process Technol 213(5):671–684
10. Afazov SM, Ratchev SM, Segal J et al (2012) Chatter modeling in micro-milling by considering process nonlinearities. Int J Mach Tools Manuf 56:28–38
11. Mascardelli BA, Park SS, Freiheit T (2008) Substructure coupling of microend mills to aid in the suppression of chatter. J Manuf Sci Eng 130(1):119–129
12. Mancisidor I, Urkiola A, Barcena R et al (2014) Receptance coupling for tool point dynamic prediction by fixed boundaries approach. Int J Mach Tools Manuf 78:18–29
13. Singh KK, Kartik V, Singh R (2015) Modeling dynamic stability in high-speed micromilling of Ti-6Al-4V via velocity and chip load dependent cutting coefficients. Int J Mach Tools Manuf 96:56–66
14. Song QH, Liu ZQ, Shi ZY (2014) Chatter stability for micro-milling processes with flat end mill. Int J Adv Manuf Technol 71(5–8):1159–1174
15. Schmitz TL, Donalson RR (2000) Predicting high-speed machining dynamics by substructure analysis. CIRP Ann Manuf Technol 49(1):303–308
16. Altintas Y, Budak E (1995) Analytical prediction of stability lobes in milling. Ann CIRP 44(1):357–362
17. Altintas Y (2000) Manufacturing automation: principles of metal cutting and machine tool vibrations. Cambridge University Press, Cambridge
18. Documentation, Abaqus, and User Manual (2010) Version 6.10. Dassault systemes
19. Simulia D (2011) Abaqus 6.11 theory manual. DS SIMULIA Corp., Providence
20. Schmitz TL, Smith KS (2008) Machining dynamics frequency response to improved productivity. Springer, Berlin
21. Singh KK, Singh R, Kartik V (2015) Comparative study of chatter detection methods for high-speed micromilling of Ti6Al4V. Procedia Manuf 1(1):593–606
22. Singh KK, Kartik V, Singh R (2017) Modeling of dynamic instability via segmented cutting coefficients and chatter onset detection in high-speed micromilling of Ti6Al4V. J Manuf Sci Eng 139(5):051005